ATMOSPHERIC SCIENCE LETTERS
Atmos. Sci. Let. **10**: 1–8 (2009)
Published online 23 January 2009 in Wiley InterScience
(www.interscience.wiley.com) **DOI:** 10.1002/asl.210

RMetS
Royal Meteorological Society

The role of air turbulence in warm rain initiation

Lian-Ping Wang[1]* and Wojciech W. Grabowski[2]

[1]*Department of Mechanical Engineering, 126 Spencer Laboratory, University of Delaware, Newark, Delaware 19716, USA*
[2]*Mesoscale and Microscale Meteorology Division, National Center for Atmospheric Research, PO Box 3000, Boulder, Colorado 80307, USA*

**Correspondence to:*
Lian-Ping Wang, Department of Mechanical Engineering, 126 Spencer Laboratory, University of Delaware, Newark, Delaware 19716-3140.
E-mail: lwang@udel.edu

Received: 14 August 2008
Revised: 7 December 2008
Accepted: 7 December 2008

Abstract

Quantitative parameterization of turbulent collision of cloud droplets represents a major unsolved problem in cloud physics. Here a hybrid direct simulation tool is used specifically to quantify the turbulent enhancement of the gravitational collision-coalescence. Simulation results show that air turbulence can enhance the collision kernel by an average factor of about 2, and the observed trends are supported by scaling arguments. An impact study using the most realistic collection kernel suggests that cloud turbulence can significantly reduce the time for warm rain initiation. Areas for further development of the hybrid simulation and the impact study are indicated. Copyright © 2009 Royal Meteorological Society

Keywords: **collision-coalescence; cloud microphysics; turbulence; warm rain development**

1. Introduction

Atmospheric clouds dominate the visual appearance of Earth when viewed from space. While visible clouds may extend over distances up to hundreds of kilometers, the individual water droplets are typically only 5 to 20 μm in radius. In warm (i.e. above-freezing) clouds, droplets may further grow by collision-coalescence to form drizzle droplets or raindrops, typically a few hundred microns to several millimeters in diameter. Rainfall produced in such a way (referred to as 'warm rain', in contrast to precipitation formed by ice processes) accounts for about 30% of the total rainfall on the planet and roughly 70% of the total rain area in the tropics (Lau and Wu, 2003). In general, global radiative and hydrological fluxes are strongly linked to microphysical processes in clouds (Baker, 1997) which determine, among other things, the number concentration and size distribution of cloud droplets. Representation of cloud microphysical processes is a source of significant uncertainty in numerical weather prediction and climate models. Critical weather phenomena such as aircraft icing and freezing precipitation often result from warm rain processes, sometimes with deadly consequences (Marwitz *et al*., 1997; Huffman and Norman, 1988).

Small cloud droplets (i.e. radii less than roughly 15 μm) grow efficiently by the diffusion of water vapor; they are unable to grow efficiently by gravitational collisions until their radius reaches about 50 μm (Pruppacher and Klett, 1997). In general, it is difficult to explain the rapid growth in cloud droplets in the size range from 15 to 50 μm in radius for which neither the diffusional mechanism nor the gravitational collision-coalescence mechanism is effective (i.e. the condensation-coalescence bottleneck). An open question is what drives the droplet growth through the bottleneck size range. The onset of drizzle-size drops (∼100 μm in radius) is still poorly understood, and this issue is regarded as one of the important unresolved problems of cloud physics. A related issue is the discrepancy between the width of observed and simulated size distributions of cloud droplets (Brenguier and Chaumat, 2001).

Several mechanisms have been proposed to explain the rapid development of rain in shallow convective clouds, including entrainment of dry environmental air into the cloud, effects of giant aerosol particles, turbulent fluctuations of the water vapor supersaturation, and turbulent collision-coalescence (Pruppacher and Klett, 1997; Xue *et al*., 2008). A review of these issues and related references can be found in Wang *et al*. (2006); Xue *et al*. (2008). Here we focus on the effects of air turbulence on the growth of cloud droplets by collision-coalescence. The central issue is the magnitude of the enhancement of the gravitational collection kernel due to the air turbulence, and whether the enhancement can significantly impact rain initiation. We will show that, despite the complexity of the problem, recent quantitative studies begin to address these long-standing issues with confidence.

2. Turbulent collision-coalescence

During the last 15 years, an increasing number of studies have emerged in both engineering and atmospheric literature concerning the collision rate of inertial particles in turbulent flow (see Xue *et al*. (2008) for relevant references). These studies suggest that the collection kernel of cloud droplets could be enhanced by several effects of air turbulence: (1) the enhanced relative motion due to differential acceleration and shear effects; (2) the enhanced average pair density

due to local clustering or preferential concentration of droplets; (3) the enhanced settling rate; and (4) the enhanced collision efficiency. The enhancement depends, in a complex manner, on the size of droplets (which in turn determines the response time and terminal velocity) and the strength of air turbulence (i.e. the dissipation rate, flow Reynolds number, etc.).

Owing to the relatively low flow dissipation rate in clouds, the collision-coalescence of cloud droplets tends to be governed by the gravitational settling and dissipation-range scales of the air turbulence. The two key physical parameters are the droplet inertial response time τ_p and the still-fluid droplet terminal velocity v_T. The dissipation-range air turbulence are characterized by the Kolmogorov time τ_k and the Kolmogorov velocity v_k. The Stokes number St, the ratio τ_p/τ_k, emphasized in early studies of particle-laden flows, is not the only parameter governing the interaction of droplets with air turbulence. The nondimensional settling velocity, $S_v \equiv v_T/v_k$, is the second key parameter, typically one order of magnitude larger than St (Grabowski and Vaillancourt, 1999). This implies that the gravitational sedimentation determines the interaction time between the cloud droplet and the small-scale flow structures. Most of the published results on droplet clustering and collision rate from numerical simulations and theoretical studies assume no sedimentation and, as such, are not directly applicable to cloud droplets.

Recent systematic studies of the collection kernel for cloud droplets have been undertaken through either direct numerical simulation (DNS) (Wang *et al*., 2005, 2008; Franklin *et al*., 2007; Ayala *et al*., 2008b) or a kinematic/stochastic representation of turbulence (Pinsky *et al*., 1999, 2006). These studies provide not only quantitative data on the turbulent collision kernel, but also reveal that turbulent collisions of cloud droplets are dynamic events in a complex multiphase flow system affected by a range of scales from those governing the background air turbulence to those characterizing droplet–droplet aerodynamic interactions.

In parallel, several attempts have been made to address the impact of selected aspects of air turbulence on the time evolution of the droplet size spectrum. It has been demonstrated that collection kernels taking into account the effect of air turbulence on relative motion of droplets can lead to the acceleration of large droplet and raindrop formation (Pinsky and Khain, 2002). The analysis in Falkovich *et al*. (2002) implies that preferential concentration of droplets and local fluid acceleration due to cloud turbulence can substantially accelerate the formation of large droplets that trigger rain. Another analysis (Ghosh *et al*., 2005) illustrates that the selectively enhanced settling velocity due to air turbulence could make droplets grow rapidly from 20 to 80 μm and that this mechanism does not depend on the level of cloud turbulence. These studies, however, are based on turbulent collection kernels derived from either approximate or empirical formulations of the air turbulence and/or the motion of cloud droplets and, consequently, should be treated as primarily being qualitative. In two very recent studies, more realistic turbulent collision kernels derived from DNSs were applied to study the growth of cloud droplets (Xue *et al*., 2008) and warm rain parameterization in terms of conversion rates from cloud droplets to rain drops (Franklin, 2008). These studies demonstrated a significant reduction in warm rain initiation time when the turbulent collision kernel was used in place of the gravitational collision kernel, and the level of the reduction increases with air flow dissipation rate. In these two studies, a turbulence geometric collision kernel with gravitational collision efficiencies was employed. Here we will extend the calculations of Xue *et al*. (2008) to include turbulent collision efficiencies.

3. Hybrid simulation approach

Motivated by the issues explained above, we have developed a consistent and rigorous simulation approach to the problem of turbulent collisions of cloud droplets (Wang *et al*., 2005; Ayala *et al*., 2007). The basic idea of the approach is to combine DNS of the background air turbulence with an analytical representation of the disturbance flow introduced by droplets (Figure 1). The approach takes advantage of the fact that the disturbance flow due to droplets is localized in space and there is a sufficient length-scale separation between the droplet size and the Kolmogorov scale of the background turbulent flow. This hybrid approach provides, for the first time, a quantitative tool for studying the combined effects of air turbulence and aerodynamic interactions on the motion and collisional interactions of cloud droplets. The disturbance flow is coupled with the background air turbulence through the approximate implementation of the nonslip boundary conditions on each droplet. Both the near-field and the far-field droplet–droplet aerodynamic interactions could be incorporated (Wang *et al*., 2007b), with possible systematic improvements of their accuracy.

The most important aspect of the approach is that dynamic collision events are detected, along with the direct and consistent calculations of all kinematic pair statistics related to the collision rate (Wang *et al*., 2005). These unique capabilities help establish the following general kinematic formulation of the collection kernel K_{12} (Sundaram and Collins, 1997; Wang *et al*., 2005)

$$K_{12} = 2\pi R^2 \langle |w_r(r = R)| \rangle g_{12}(r = R) \qquad (1)$$

where the geometric collision radius R is defined as $R = a_1 + a_2$, with a_1 and a_2 being the radii of the two colliding droplets, w_r is the radial relative velocity at contact which combines the differential sedimentation and turbulent transport, and g_{12} is the radial distribution function (RDF) that quantifies the effect of droplet-pair clustering on the collision rate.

DOI: 10.1002/asl

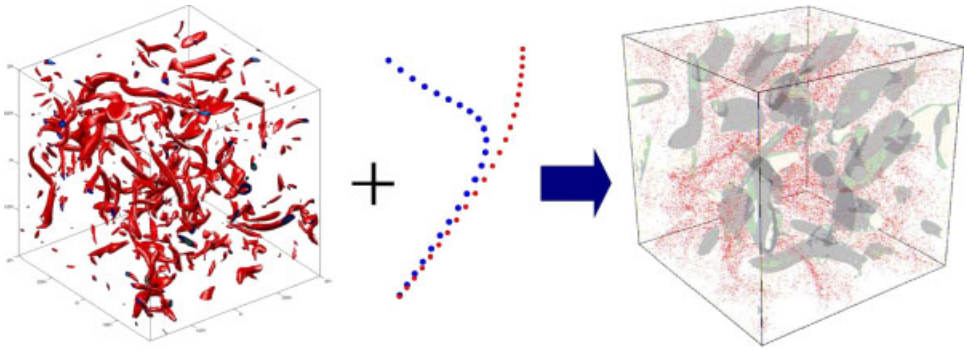

Figure 1. Visualizations from the hybrid simulation approach. The left panel shows vortical structures of the background air turbulence; the center panel shows trajectories of two colliding droplets at the scale of droplets in the turbulent flow; and the right panel is a snapshot of flow vorticity surfaces and the locations of droplets in a subdomain of the computational region.

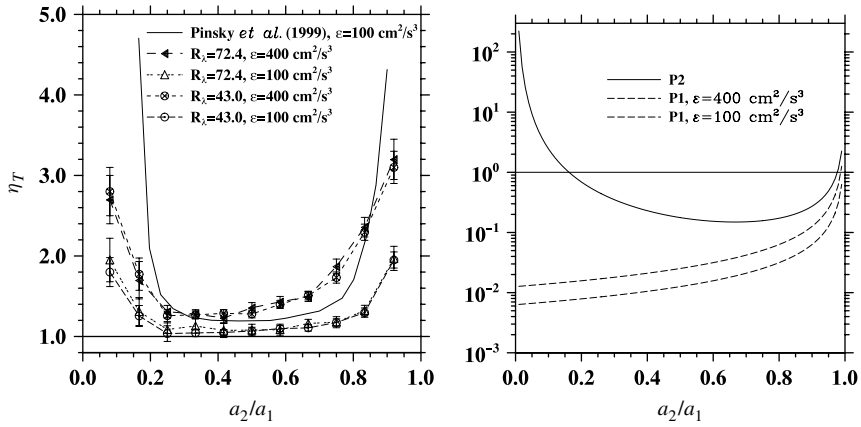

Figure 2. Left panel: The net enhancement factor, the ratio of the turbulent collection kernel and the hydrodynamic-gravitational collection kernel, is plotted as a function of the radius ratio a_2/a_1, with the larger droplet at 30 μm in radius. In the legend, ϵ is the flow viscous dissipation rate and R_λ is the Taylor microscale Reynolds number of the simulated background turbulent air flow. Right panel: The two scale ratios P_1 and P_2 defined in Equations (2) and (3) as a function of a_2/a_1 with $a_1 = 30$ μm.

Saw *et al.* (2008) have recently obtained convincing experimental evidence of droplet-pair clustering in high-Reynolds-number turbulence, with results in quantitative agreement with published theoretical and numerical results. The above formulation is applicable to aerodynamically interacting droplets in a turbulent background flow, showing that the total enhancement factor η_T of the collision rate is a product of the enhancement of the geometric collision, η_G, and the enhancement of the collision efficiency, η_E.

4. Turbulent enhancement

This section highlights selected findings obtained using the hybrid DNS approach. Figure 2 shows the net enhancement factor $\eta_T = \eta_E \eta_G$ by air turbulence as a function of a_2/a_1 for $a_1 = 30$ μm. To interpret the shape of η_T, we first note that air turbulence is only effective in altering the local aerodynamic interaction when either (1) the level of turbulent fluctuations at the scale of R is at least comparable to the differential terminal velocity $(v_{T1} - v_{T2})$, or (2) the aerodynamic interaction time $[\sim R/(v_{T1} - v_{T2})]$ is of the order of τ_{p2}, the inertial response time of the smaller droplet. The first condition may be stated as

$$P_1 \equiv \frac{R(v_k/\eta)}{v_{T1} - v_{T2}} = \frac{9}{2}\frac{\rho}{\rho_w}\frac{\sqrt{\epsilon\nu}}{(a_1 - a_2)|\mathbf{g}|} \geq C_1 \qquad (2)$$

where ϵ is the mean viscous dissipation rate of the turbulence, ν is the air kinematic viscosity, ρ is air density, ρ_w is water density, $\mathbf{g}$ is the gravitational acceleration, and C_1 is a constant of the order of one. Therefore, this first condition prefers a larger ϵ and a value of a_2/a_1 close to one. The second condition may be stated as

$$P_2 \equiv \frac{R}{(v_{T1} - v_{T2})\tau_{p2}} = \left(\frac{9}{2}\frac{\rho}{\rho_w}\right)^2 \frac{\nu^2/|\mathbf{g}|}{a_2^2(a_1 - a_2)} \geq C_2 \qquad (3)$$

which favors the two limiting cases of $a_2/a_1 \to 0$ for a given a_1, or $a_2/a_1 \to 1$. The above-scaling arguments show that a larger η_E should occur for the two limits of $a_2/a_1 \to 0$ or $a_2/a_1 \to 1$. It also follows that η_E decreases with increasing a_1 for a fixed a_2/a_1.

The right panel of Figure 2 shows the above-scale ratios as a function of a_2/a_1 for $a_1 = 30$ μm. The figure confirms that the ratios tend to be larger near the two limiting cases, with a magnitude reaching order

DOI: 10.1002/asl

of one or larger. It also shows that, in the limit of $a_2/a_1 \to 0$, the long hydrodynamic interaction time is key to the turbulence enhancement of the collision efficiency.

A similar qualitative behavior for η_G can be inferred. In this case, the first condition, Equation (2), must also be satisfied to obtain a significant η_G value. Other conditions for enhanced geometric collision through particle clustering would be $\tau_p \sim \tau_k$ (Wang and Maxey, 1993) and $F_p = {\tau_p}^3|\mathbf{g}|^2/\nu \sim 1$ (Ghosh *et al*., 2005; Ayala *et al*., 2008b). For ν=0.17 cm^2/s, $|\mathbf{g}|$=980 cm/s^2, $\rho_w/\rho \approx$1000, the condition $F_p \sim 1$ implies a droplet radius at about 21 μm, independent of the flow dissipation rate. The condition of $\tau_p \sim \tau_k$ yields a droplet radius of

$$a(\mu m) \sim \frac{177}{[\epsilon(\text{in cm}^2/\text{s}^3)]^{0.25}} \tag{4}$$

which is about 56 and 40 μm for a dissipation rate of 100 and 400 cm^3/s^2, respectively. Therefore, for a dissipation rate of 400 cm^3/s^2, we expect that the preferential concentration is most relevant for droplets in the size range from 21 to 40 μm, i.e. those in the bottleneck range. We find that η_T can typically vary from 1 to 3 when $a_2/a_1 \sim$1, for the two representative dissipation rates of 100 and 400 cm^2/s^3. The overall conclusion is that η_T is moderate but it occurs at the right places, that is, where the hydrodynamic-gravitational collection kernel tends to be relatively small. Complete compilations and discussions of the simulation results are found in Ayala *et al*. (2008b) and Wang *et al*. (2008)

5. Impact on warm rain initiation

We next consider the question of how the above turbulent enhancements on the collection kernel alter the size evolution of cloud droplets. An analytical model has been developed for the geometric collision rate of cloud droplets based on the results from the hybrid simulation approach (Ayala *et al*., 2008a). The model consists of a parameterization of the radial relative velocity $\langle w_r \rangle$ and a parameterization of the RDF g_{12}, both for sedimenting particles. Of significance is the fact that the above parameterizations for both $\langle w_r \rangle$ and g_{12} consider the effects of flow Reynolds number which cannot be fully represented by the hybrid simulations. For example, the parameterization for $\langle w_r \rangle$ makes use of velocity correlations that are valid for both the dissipation subrange and the energy-containing subrange of turbulence (Zaichik *et al*., 2003). The intermittency of small-scale turbulent fluctuations can be incorporated into the model for RDF (Chun *et al*., 2005). Therefore, our parameterization of the collection kernel, to certain extent, can represent realistic flow Reynolds numbers in clouds.

Moreover, we include the enhancement η_E on the collision efficiency by interpolating and extending the tabulated simulation results of η_E from Wang *et al*. (2008). Additional simulations at $a_2/a_1 = 0.916$ and $a_2/a_1 = 0.0835$ were also performed. Specifically, for each droplet size combination studied, η_E is obtained by dividing the turbulent collision efficiency with the collision efficiency in still air, both of which were simulated with our hybrid DNS approach as described in Wang *et al*. (2008). For the case of equal-sized pairs ($a_2/a_1 = 1$), the turbulent collision efficiency could depend on the overall droplet number concentration used (Wang *et al*., 2008), in this case, an averaged value was used. For the case of $a_2/a_1 \to 0$, we simply set η_E to be the same as the enhancement factor at $a_2/a_1 = 0.0835$, the smallest ratio simulated in our hybrid simulations. Table 1 shows the tabulated η_E values used in this study. Note that the values for $a_1 \leq 20$ μm were not simulated but were simply set to the values at $a_1 = 20$ μm; and similarly, the values at $a_1 = 50$ μm are used for $a_1 = 60$ μm. The factor η_E is set to one for $a_1 = 100$ μm or larger. The estimate of η_E used for the limit of $a_2/a_1 \to 0$ is likely a conservative one, namely, we expect the η_E factor to be larger in this limit due to extremely small collision efficiency in still air. The tabulated data are viewed as preliminary and they will be improved as both the hybrid approach is refined and more computing resources become available.

The net ratio (η_T) of the resulting turbulent collection kernel to the Hall kernel (Hall, 1980) is shown in Figure 3 for a typical condition of cloud turbulence. The Hall kernel, a hydrodynamical gravitational kernel independent of air turbulence, is used as a base to compare the relative impact of turbulence.

Table 1. The enhancement factor η_E on collision efficiency. In each case, the first number is for ϵ = 100 cm^2/s^3 and the second for ϵ = 400 cm^2/s^3

a_2/a_1	a_1 = 10 μm	20 μm	30 μm	40 μm	50 μm	60 μm	100 μm
0.0	1.74	1.74	1.773	1.49	1.207	1.207	1.0
	4.976	4.976	3.593	2.519	1.445	1.445	1.0
0.1	1.46	1.46	1.421	1.245	1.069	1.069	1.0
	2.984	2.984	2.181	1.691	1.201	1.201	1.0
0.2	1.32	1.32	1.245	1.123	1.000	1.000	1.0
	1.988	1.988	1.475	1.313	1.150	1.150	1.0
0.3	1.250	1.250	1.148	1.087	1.025	1.025	1.0
	1.490	1.490	1.187	1.156	1.126	1.126	1.0
0.4	1.186	1.186	1.066	1.060	1.056	1.056	1.0
	1.249	1.249	1.088	1.090	1.092	1.092	1.0
0.5	1.045	1.045	1.000	1.014	1.028	1.028	1.0
	1.139	1.139	1.130	1.091	1.051	1.051	1.0
0.6	1.070	1.070	1.030	1.038	1.046	1.046	1.0
	1.220	1.220	1.190	1.138	1.086	1.086	1.0
0.7	1.000	1.000	1.054	1.042	1.029	1.029	1.0
	1.325	1.325	1.267	1.165	1.063	1.063	1.0
0.8	1.223	1.223	1.117	1.069	1.021	1.021	1.0
	1.716	1.716	1.345	1.223	1.100	1.100	1.0
0.9	1.570	1.570	1.244	1.166	1.088	1.088	1.0
	3.788	3.788	1.501	1.311	1.120	1.120	1.0
1.0	20.3	20.3	14.6	8.61	2.60	2.60	1.0
	36.52	36.52	19.16	22.80	26.0	26.0	1.0

DOI: 10.1002/asl

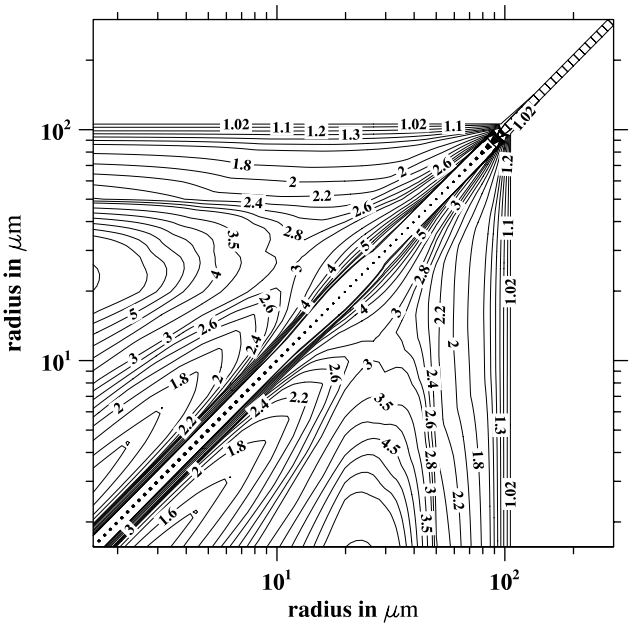

Figure 3. The ratio of a typical turbulent collection kernel to the Hall kernel. The ratio on the 45° degree line is undefined due to the zero value of the Hall kernel. The ratio is essentially one when droplets are above 100 μm. The flow dissipation rate is 400 cm^2/s^3 and rms velocity is 202 cm/s.

Several important observations can be made from Figure 3. First, a noticeable enhancement occurs for droplets less than 100 μm. Second, the overall enhancement is moderate with a value ranging from 1.0 to 4.0 for most regions or an average value of about 2 for droplets in the bottleneck size range. The net enhancement includes enhancements by air turbulence on collision efficiency, the relative velocity (i.e. the turbulent transport effect), and the droplet clustering (i.e. the accumulation effect). In general, the turbulent transport effect and turbulent efficiency dominates the net enhancement for small cloud droplets (say, less than 20 μm). For larger cloud droplets (30–60 μm), the accumulation effect and the turbulent transport effect are more important. For larger cloud droplet pairs close in size, the accumulation effect can dominate the enhancement. These have been documented and discussed in detail in Ayala *et al*. (2008b); Xue *et al*. (2008) and Wang *et al*. (2008). The enhancement factors shown in Figure 3 are similar to those reported recently in Pinsky *et al*. (2006), where dramatically different approaches were employed.

The above turbulent collection kernel is then used in the kinetic collection equation to solve for droplet size distributions at different times, starting from the initial number density distribution

$$n(x, t=0) = \frac{L_0}{\overline{x}_0{}^2} \exp\left(-\frac{x}{\overline{x}_0}\right) \tag{5}$$

where x is the droplet mass, L_0 is the liquid water content and is set to 1 g/m^3, and $\overline{x}_0$ is the initial average mass of the cloud droplets and is assumed to be 3.3×10^{-9} g which corresponds to a mean radius of 9.3 μm. The above distribution yields an initial relative radius dispersion (the ratio between the standard deviation and the mean droplet radius) of 0.36, which is within the range of 0.1–0.4 observed in stratocumulus (Pawlowska *et al*., 2006).

The kinetic collection equation is solved by an accurate method (Wang *et al*., 2007a) which combines the advantages of flux-based methods and spectral moment-based methods. A small bin mass ratio of $2^{0.25}$ ensures that the numerical solutions are free from numerical diffusion and dispersion errors. The mass distribution $g(\ln r, t) \equiv 3x^2 n(x, t)$ is usually plotted at different times in order to examine growth processes (Berry and Reinhardt, 1974). In Figure 4, we instead plot the local rate of change, $\partial g/\partial t$, as a function of radius for times from 0 to 60 min every 1 min. We compare the results using the turbulent kernel to those using the Hall kernel. The plots naturally reveal the three growth phases first described qualitatively in Berry and Reinhardt (1974): (1) *the autoconversion phase* in which self-collections of small cloud droplets near the peak of the initial size distribution slowly shift the initial peak of the distribution toward larger sizes; (2) *the accretion phase* in which the accretion mode dominates over the autoconversion mode and serves to quickly transfer mass from the initial peak to the newly formed secondary peak at drizzle sizes; and (3) *the large hydrometeor self-collection phase* in which the self-collections of drizzle droplets move the second peak toward the raindrop sizes (a few millimeters). By examining the locations corresponding to the maximum and minimum $\partial g/\partial t$, one can unambiguously identify the time intervals of the three phases (Xue *et al*., 2008). In Figure 4, we indicate in each plot the beginning and end of the accretion phase by two red horizontal lines.

Figure 4 highlights striking differences between the two collection kernels. The intensity of the autoconversion is significantly increased by the turbulent effects as shown by the magnitude of $\partial g/\partial t$ at early times (Figure 4(b)) when compared to the base case (Figure 4(a)). The time interval for the autoconversion phase *is reduced from about 32.5 min (Hall kernel) to only 10.5 min (the turbulent kernel)*. This demonstrates that turbulence has a strong impact on the autoconversion phase, which is typically the longest phase of warm rain initiation. The time interval for the accretion phase is also significantly reduced and smaller drizzle drops ($\sim$ 100 to 300 μm) are produced during this phase.

If a radar reflectivity factor of 20 dBZ (or the mass-weighted mean droplet radius of 200 μm) is used as an indicator for the drizzle precipitation, the time needed to reach such a reflectivity (or mean droplet radius) changes from about 2450 s (or 2470 s) for the Hall kernel to 1230 s (or 1250 s) for the turbulent kernel. This twofold reduction factor increases with either the dissipation rate or rms turbulent fluctuation velocity (Xue *et al*., 2008).

DOI: 10.1002/asl

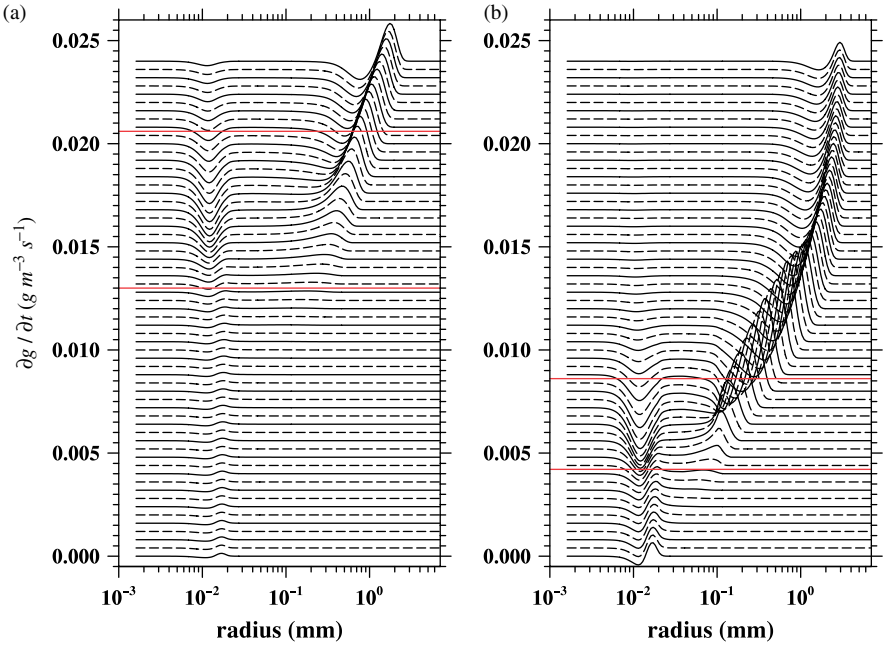

Figure 4. The rate of change ($\partial g/\partial t$, g m^{-3} s^{-1}) of droplet mass density in each numerical bin as a function of droplet radius: (a) solutions using the Hall kernel; (b) solutions using a turbulent kernel at flow dissipation rate of 400 cm^2/s^3 and root mean square (rms) fluctuation velocity of 2.0 m/s. There are 61 curves in each plot, representing $t = 0$ to $t = 60$ min with a time increment of 1 min. The curves for $t > 0$ is shifted upwards by a constant in order to distinguish them. The value of $\partial g/\partial t$ can be either positive or negative, with the total integral over the whole size range equal to zero due to the mass conservation. At any given time, a positive $\partial g/\partial t$ for a given size bin implies that the mass density for that size bin is increasing. The two red lines mark the beginning and the end of the accretion phase.

Finally, in Figure 5 we illustrate how the time needed to reach the accretion phase depends on the collection kernel and the width of the initial size distribution. For this purpose, the following generalized initial number density distribution is considered:

$$n(x, t=0) = A\frac{L_0}{\overline{x}_0{}^2}\exp\left[-\left(\frac{Bx}{\overline{x}_0}\right)^{\alpha}\right] \qquad (6)$$

where α is varied to produce different initial radius dispersions, and two constants A and B are specified such that the physical interpretations of $\overline{x}_0$ and L_0 are unchanged. The relative radius dispersion γ is defined as the ratio between the standard deviation of droplet radius and the mean radius. The case of $\alpha = A = B = 1$ is the reference case considered above (Case 1), yielding $\gamma = 0.3634 \equiv \gamma_0$. Two other cases with smaller initial radius dispersions are also considered: Case 2 has $\alpha = 2$, $A = 0.636618$, $B = 0.564189$, which gives $\gamma = 0.3015$. Case 3 has $\alpha = 3$, $A = 0.566034$, $B = 0.505479$, which results in $\gamma = 0.2825$. A total of nine simulations were performed, using different combinations of the initial radius dispersion, the collection kernel type, and the level of flow dissipation rate. The two simulations shown in Figure 4 are two of the nine runs shown in Figure 5. The line fit in Figure 5 represents as below

$$T_A \approx 0.08 \times \left(\frac{\partial g(\ln r, t=0)}{\partial t}\right)^{-2/3}_{\max} \times \left(\frac{\gamma}{\gamma_0}\right)^{-4} \qquad (7)$$

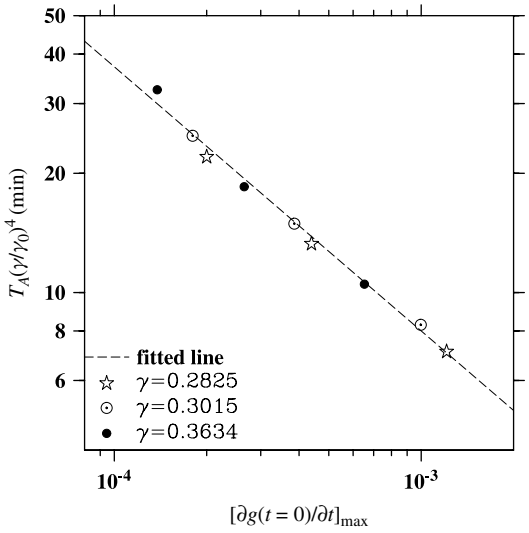

Figure 5. The transition time (T_A) from the autoconversion phase to the accretion phase, after empirically adjusted for the initial relative radius dispersion, plotted as a function of the maximum magnitude of $\partial g/\partial t$ at $t = 0$. The flow rms fluctuation velocity is set to 2.0 m/s. Three different symbols represent three different initial radius dispersions. For each γ, the three data points correspond to, from left to right, the Hall kernel, the turbulent collection kernel with $\epsilon = 100$ cm^2/s^3, and the turbulent collection kernel with $\epsilon = 400$ cm^2/s^3.

The excellent fit shows that the transition time T_A from the autoconversion phase to the accretion phase depends primarily on two properties, the initial dispersion γ and the initial autoconversion intensity as

DOI: 10.1002/asl

measured by the maximum $\partial g/\partial t$ at $t = 0$. Despite the very strong nonlinearity for the autoconversion phase, the above correlation demonstrates a surprisingly simple picture: the rain initiation time is shortened by either increasing the initial radius dispersion γ or increasing the initial autoconversion rate. The latter can be accomplished by turbulent enhancements discussed in this paper. The former may be a result from different characteristics of the cloud condensation nuclei (CCN; Blyth *et al*. (2003). The two different mechanisms are brought together within the above unified framework for studying the rain initiation processes.

6. Summary and conclusions

Studies during the last 10 years have significantly advanced our understanding of the effects of cloud turbulence on the collision-coalescence of cloud droplets. There is a sufficient evidence that the air turbulence accelerates the development of drizzle and rain precipitation. Meanwhile, much work is still needed to bring the research in this area to the level of quantitative science. Our systematic efforts to remove uncertainties have led us to conclude that the enhancement factor by the air turbulence is moderate, which further implies the importance of quantitative measures and the need for rigorous research methodologies. The hybrid DNS approach represents the first step in this direction. Current limitations of our hybrid DNS approach and on-going efforts to address these limitations are discussed in Ayala *et al*. (2008b); Wang *et al*. (2008). The challenging issues from the perspective of collection kernel parameterization include characterization of RDF, flow Reynolds-number effects, and the modeling of droplet–droplet short-range interactions (Ayala *et al*., 2008a,b; Wang *et al*., 2008).

Our results advance the current understanding of the growth processes during the warm rain initiation. Since the moderate enhancements by air turbulence occur within the bottleneck range and since the autoconversion is the longest phase of the initiation process, there is now convincing evidence showing that turbulence plays a definite role in promoting rain formation. Recently, a rising adiabatic parcel model has been used to extend the impact study shown here by combining droplet activation, diffusional growth and turbulent collision-coalescence (Grabowski and Wang, 2008). Using the same turbulent collection kernel, it has been shown that the warm rain initiation time is reduced by 25 to 40%, demonstrating the important role of air turbulence in a more realistic warm rain model.

The mechanism discussed here does not exclude other mechanisms that may promote even more rapid rain initiation. In general, these mechanisms may operate simultaneously in the same part of a cloud, or they may act separately in different regions. For instance, both entrainment-mixing and turbulent collisions are expected to promote droplet growth near cloud edges where the cloud water content is reduced but the width of the droplet spectrum and the turbulence intensity are increased. In the core region, where the turbulence intensity is typically lower but the cloud water content is high, the turbulent mechanism can operate jointly with the giant aerosol mechanism, if such aerosol particles are part of the CCN spectrum. These aspects will need to be investigated in the future when the developments discussed in this paper are incorporated into dynamic models of warm precipitating clouds.

Finally, no attempt was made here to compare our simulated droplet size distribution with observations when turbulence enhanced collision kernels were used. In the calculations of droplet size distribution shown in this paper, an idealized initial droplet size distribution was assumed and only the growth by collision-coalescence was considered (i.e. droplet activation and diffusional growth were excluded). Therefore, it is not yet appropriate to compare the droplet spectra from real clouds to our idealized calculations here. A parcel model approach considering activation, condensational growth and collision-coalescence together has been presented in Grabowski and Wang (2008), using the same turbulent collision kernel. But even with this parcel model, there are several assumptions/simplifications (e.g. issues with activation modeling, sedimentation, constant updraft velocity and lack of entrainment) that make it difficult to compare the simulated spectra with observations. At this stage, the simplicity of our modeling approach and the complications in real clouds do not allow a direct and meaningful comparison.

Acknowledgements

This work was supported by the National Science Foundation (NSF) under grants ATM-0114100 and ATM-0527140. LPW also acknowledges support by the NSF Grant No. PHY05-51164 through Kavli Institute for Theoretical Physics at UCSB, and by National Natural Science Foundation of China (Project No. 10628206). WWG acknowledges additional support from NOAA grant NA05OAR4310107. Various contributions to this research were made by Dr O. Ayala, Dr Y. Xue, and Dr B. Rosa.

References

Ayala O, Rosa B, Wang L-P. 2008a. Effects of turbulence on the geometric collision rate of sedimenting droplets: Part 2. Theory and parameterization. *New Journal of Physics* **10**: 075016, Doi: 10.1088/1367-2630/10/7/075016.

Ayala O, Rosa B, Wang L-P, Grabowski WW. 2008b. Effects of turbulence on the geometric collision rate of sedimenting droplets: Part 1. Results from direct numerical simulation. *New Journal of Physics* **10**: 075015, Doi:10.1088/1367-2630/10/7/075015.

Ayala O, Wang L-P, Grabowski WW. 2007. A hybrid approach for simulating turbulent collisions of hydrodynamically-interacting particles. *Journal of Computational Physics* **225**: 51–73.

Baker MB. 1997. Cloud microphysics and climate. *Science* **276**: 1072–1078.

DOI: 10.1002/asl

Berry EX, Reinhardt RI. 1974. An analysis of cloud drop growth by collection: Part I. Double distributions. *Journal of the Atmospheric Sciences* **31**: 1814–1824.

Blyth AM, Lasher-Trapp SG, Cooper WA, Knight CA, Latham J. 2003. The role of giant and ultragiant nuclei in the formation of early radar echoes in warm cumulus clouds. *Journal of the Atmospheric Sciences* **60**: 2557–2572.

Brenguier J-L, Chaumat L. 2001. Droplet spectra broadening in cumulus clouds. Part I: Broadening in adiabatic cores & Part II: Microscale droplet concentration heterogeneities. *Journal of the Atmospheric Sciences* **58**: 628–654.

Chun J, Koch D, Rani SL, Ahluwalia A, Collins LR. 2005. Clustering of aerosol particles in isotropic turbulence. *Journal of Fluid Mechanics* **536**: 219–251.

Falkovich G, Fouxon A, Stepanov MG. 2002. Acceleration of rain initiation by cloud turbulence. *Nature* **419**: 151–154.

Franklin CN. 2008. A warm rain microphysics parameterization that includes the effect of turbulence. *Journal of the Atmospheric Sciences* **65**: 1795–1816.

Franklin CN, Vaillancourt PA, Yau MK. 2007. Statistics and parameterizations of the effect of turbulence on the geometric collision kernel of cloud droplets. *Journal of the Atmospheric Sciences* **64**: 938–954.

Ghosh S, Davila J, Hunt JCR, Srdic A, Fernando HJS, Jonas P. 2005. How turbulence enhances coalescence of settling particles with applications to rain in clouds. *Proceedings of the Royal Society of London A* **461**: 3059–3088.

Grabowski WW, Vaillancourt P. 1999. Comments on "Preferential concentration of clouds droplets by turbulence: Effects on the early evolution of cumulus cloud droplet spectra". *Journal of the Atmospheric Sciences* **56**: 1433–1436.

Grabowski WW, Wang L-P. 2008. Diffusional and accretional growth of water drops in a rising adiabatic parcel: effects of the turbulent collision kernel. *Atmospheric Chemistry and Physics Discussions* **8**: 14717–14763.

Hall WD. 1980. A detailed microphysical model within a twodimensional dynamic framework: Model description and preliminary results. *Journal of the Atmospheric Sciences* **37**: 2486–2507.

Huffman GJ, Norman GA. 1988. The supercooled warm rain process and the specification of freezing precipitation. *Monthly Weather Review* **116**: 2172–2182.

Lau KM, Wu H-T. 2003. Warm rain processes over tropical oceans and climate implications. *Geophysical Research Letters* **30**: Art. No. 2290. DOI:10.1029/2003GL018567.

Marwitz J, Politovich M, Bernstein B, Ralph F, Neiman P, Ashenden R, Bresch J. 1997. Meteorological conditions associated with the ATR72 aircraft accident near Roselawn, Indiana, on 31 October 1994. *Bulletin of the American Meteorological Society* **78**: 41–52.

Pawlowska H, Grabowski WW, Brenguier J-L. 2006. Observations of the width of cloud droplet spectra in stratocumulus. *Geophysical Research Letters* **33**: L19810, Doi:10.1029/2006GL026841.

Pinsky MB, Khain AP. 2002. Effects of in-cloud nucleation and turbulence on droplet spectrum formation in cumulus clouds. *Quarterly Journal of the Royal Meteorological Society* **128**: 501–533.

Pinsky MB, Khain AP, Grits B, Shapiro M. 2006. Collisions of small drops in a turbulent flow. Part III: Relative droplet fluxes and swept volumes. *Journal of the Atmospheric Sciences* **63**: 2123–2139.

Pinsky MB, Khain AP, Shapiro M. 1999. Collisions of small drops in a turbulent flow. Part I: Collision efficiency. Problem formulation and preliminary results. *Journal of the Atmospheric Sciences* **56**: 2585–2600.

Pruppacher HR, Klett JD. 1997. *Microphysics of Clouds and Precipitation*. Kluwer Academic Publishers: Dordrecht/Boston/London; 954.

Saw EW, Shaw RA, Ayyalasomayajula S, Chuang PY, Gylfason A. 2008. Inertial clustering of particles in high-Reynolds-number turbulence. *Physical Review Letters* **100**: 214501.

Sundaram S, Collins LR. 1997. Collision statistics in an isotropic particle-laden turbulent suspension. Part 1. Direct numerical simulations. *Journal of Fluid Mechanics* **335**: 75–109.

Wang L-P, Ayala O, Kasprzak SE, Grabowski WW. 2005. Theoretical formulation of collision rate and collision efficiency of hydrodynamically interacting cloud droplets in turbulent atmosphere. *Journal of the Atmospheric Sciences* **62**: 2433–2450.

Wang L-P, Maxey MR. 1993. Settling velocity and concentration distribution of heavy particles in homogeneous isotropic turbulence. *Journal of Fluid Mechanics* **256**: 27–68.

Wang L-P, Xue Y, Ayala O, Grabowski WW. 2006. Effects of stochastic coalescence and air turbulence on the size distribution of cloud droplets. *Atmospheric Research* **82**: 416–432, Doi:10.1016/j.atmosres.2005.12.011.

Wang L-P, Xue Y, Grabowski WW. 2007a. A bin integral method for solving the kinetic collection equation. *Journal of Comparative Physiology* **226**: 59–88.

Wang L-P, Ayala O, Grabowski WW. 2007b. Effects of aerodynamic interactions on the motion of heavy particles in a bidisperse suspension. *Journal of Turbulence* **8.1**: 1–23, DOI: 10.1080/14685240701233426.

Wang L-P, Ayala O, Rosa B, Grabowski WW. 2008. Turbulent collision efficiency of heavy particles relevant to cloud droplets. *New Journal of Physics* **10**: 075013, Doi:10.1088/1367-2630/10/7/075013.

Xue Y, Wang L-P, Grabowski WW. 2008. Growth of cloud droplets by turbulent collision-coalescence. *Journal of the Atmospheric Sciences* **65**: 331–356.

Zaichik LI, Simonin O, Alipchenkov VM. 2003. Two statistical models for predicting collision rates of inertial particles in homogeneous isotropic turbulence. *Physics of Fluids* **15**: 2995–3005.

DOI: 10.1002/asl